Eur. J. Mineral., 38, 179–195, 2026
https://doi.org/10.5194/ejm-38-179-2026

European Journal of Mineralogy
Open Access

Hydrous partial melting in gabbros drilled at the Southwest Indian Ridge (ODP Hole 735B): evidence from microstructures at grain boundaries

Jürgen Koepke

Leibniz University Hannover, Institute of Earth System Sciences, Callinstrasse 3, 30167 Hannover, Germany

Correspondence: Jürgen Koepke (koepke@mineralogie.uni-hannover.de)

Received: 3 October 2025 – Revised: 15 February 2026 – Accepted: 22 February 2026 – Published: 9 April 2026

Abstract. The Atlantis Bank at the Southwest Indian Ridge (SWIR) is probably the most thoroughly investigated oceanic core complex from a typical slow-spreading ridge. Here, ODP (Ocean Drilling Program) conducted two drilling expeditions at Drill Site 735B. The gabbro massif is characterized by the presence of hundreds of felsic veins, which are rocks consisting of evolved, silica-rich material showing the composition of typical "oceanic plagiogranites". Two models have been suggested for their generation: (1) the extreme differentiation of a MORB magma, resulting in a highly differentiated melt, and (2) the hydrous remelting of gabbroic rocks in the deep oceanic crust.

Detailed petrographical and microanalytical investigations of gabbroic rocks from ODP drill core 735B reveal that many of these gabbros exhibit microstructures characteristic of hydrous partial melting of gabbro. Key features that led to this conclusion are zones of anorthite-enriched plagioclase on grain boundaries, which form parageneses with interstitial brown amphibole and orthopyroxene. These are interpreted as the residual phase assemblage left after hydrous partial melting. These events are triggered by water-rich fluids migrating along grain boundaries within the cooling gabbro complex at temperatures above the wet gabbro solidus. This conclusion is supported by two further observations: (1) trace element concentrations in the An-enriched plagioclase (Ti, Mg, and K) are strongly impoverished, in line with experiments simulating the hydrous partial melting of gabbro. (2) The bulk TiO_2 content of the felsic veins shows characteristically low concentrations, consistently with an origin through the melting of TiO_2-impoverished cumulate gabbro. This contrasts with melt compositions derived through fractional crystallization of MORB, where TiO_2 concentrations are significantly higher. Our results show that hydrous partial melting of gabbro played a role in the formation of the felsic melts, alongside fractional crystallization, which is the standard model for felsic vein formation evidenced by several papers.

1 Introduction

1.1 Production of felsic melt in the deep oceanic crust of slow-spreading ridges

Only at slow-spreading ridges are centimeter- to decimeter-sized veins of SiO_2-enriched rocks known. These are often called "oceanic plagiogranites" (see Koepke et al., 2007, for definition) or "felsic veins", cutting the lower gabbroic crust in many places. These rocks generally account for less than 1 vol % of the crust (see Koepke et al., 2007, for details). The best example of such felsic veins from slow-spreading ridge systems is the gabbroic oceanic core complex "Atlantis Bank" at the Southwest Indian Ridge (SWIR, Fig. 1), where ODP (Ocean Drilling Program) and IODP (International Ocean Discovery program) drilled cores at three different sites (see the review of Dick et al., 2019). The longest drill core was drilled at Site 735B between 1987 and 1998, encountering ∼ 1.5 km of gabbroic rocks, which are cut by hundreds of igneous felsic veins, consisting of diorite, tonalite, and trondhjemite (Dick et al., 2000). Two models have been suggested for the generation of felsic veins in gabbroic complexes from slow-spreading ridges: (1) crystal fractionation in MORB magmas, resulting in highly differ-

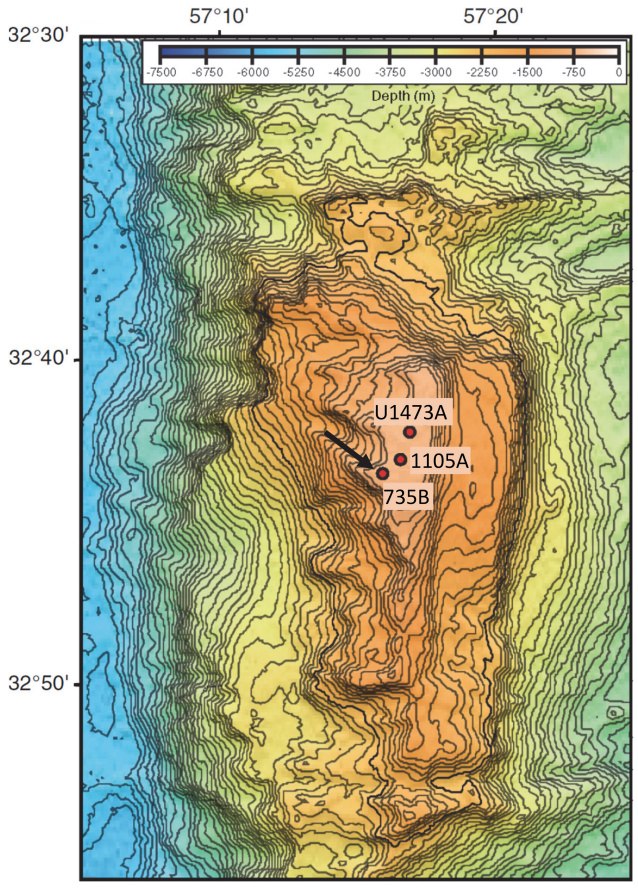

Figure 1. Bathymetry of the Atlantis Bank at the SWIR, including the ODP and IODP drill sites. The drilled gabbros from this study are from Hole 735B (marked by an arrow). Modified after Dick et al. (2016).

entiated melt (e.g., Berndt et al., 2005; Niu et al., 2002; Chen et al., 2019; Zhang et al., 2025), and (2) hydrous remelting of gabbroic rocks in the deep oceanic crust (e.g., Flagler and Spray, 1991; Brophy and Pu, 2012; Koepke et al., 2004, 2007; Zhang et al., 2025). Both models have been verified by experimental studies (e.g., Berndt et al., 2005; Koepke et al., 2004; Wolff et al., 2013).

With regard to model 2, the corresponding experiments on hydrous partial melting of gabbro were conducted using natural starting material and significantly different grain sizes. While Koepke et al. (2004) used very fine-grained material to achieve global equilibrium conditions, Wolff et al. (2013) used microrocks of the same gabbro to shed light on the kinetics of the partial-melting process. Although far from global equilibrium, the observed phase relations and compositional trends in the microrock experiment results are practically identical to those in runs using a very fine-grained powder. This provides a detailed insight into the reaction kinetics (Wolff et al., 2013). Interestingly, textural features and compositional characteristics obtained in the partial-melting experiments on microrocks are in good agreement with corresponding features of interstitial assemblages in some natural oceanic gabbros from slow-spreading ridges. This suggests that some natural late-stage parageneses may be better explained as residual phases left behind after a hydrous partial-melting event rather than by the crystallization of a late, evolved percolating melt.

1.2 Gabbros hosting felsic veins from the Atlantis Bank at the SWIR

Two longer cores were drilled at the top of the Atlantis Bank: Hole 735B (ODP Legs 118 and 176), which was drilled between 1987 and 1998 (see Dick et al., 2000, for details), and Hole U1473A, which was drilled by IODP Expedition 360 in 2016 (for details, see MacLeod et al., 2017; Dick et al., 2019; Fig. 1). Comparing the two drilling processes demonstrates continuity in both holes, emphasizing the complex interplay of magmatic accretion and steady-state detachment faulting over a period of $\sim$ 128 kyr (MacLeod et al., 2017). The results show that the lower crust of the Atlantis Bank was built up through repeated cycles of intrusion by several bodies of olivine gabbro, each hundreds of meters in size.

Several dozen publications on the gabbro rocks drilled in both holes provide a foundation of knowledge on how the deep oceanic crust under slow-spreading ridges is formed. The gabbros from both drill cores are composed of a variety of gabbroic lithologies, from primitive olivine gabbros to evolved oxide-rich gabbros, cut by hundreds of millimeter- to centimeter-thick felsic veins (Dick et al., 2000; MacLeod et al., 2017). Examples of findings relating to gabbros drilled in Hole 735B can be found in the work of Natland et al. (1991) and Dick et al. (2000, 2002). Several publications focusing on gabbros from Hole U1473A over the last 7 years demonstrate the geoscience community's general interest in the Atlantis Bank gabbros. Petrological studies focusing on magma formation and evolution show that "simple" fractional crystallization is not the main process behind the formation of crustal magmas. Instead, the importance of other processes is emphasized: assimilation/fractional crystallization as the key mechanism in lower crust formation (Dhar et al., 2022), the role of compaction in melt extraction and accumulation (Ferrando et al., 2021), the pervasive reactive transport of ferrobasaltic melts formed during early crystallization of Fe–Ti oxides as monitored by amphibole geochemistry (Ferrando et al., 2022), melt rock reaction by the intergranular reactive porous flow of a melt migrating through the mush framework (Sanfilippo et al., 2020), processes controlling halogen (F, Cl, Br, I) abundances (Kendrick, 2019), the importance of melt migration by intrusion processes or porous flow at all scales (Boulanger et al., 2021), the role of multi-stage melt migration due to compaction and syn-magmatic deformation during crustal accretion (Zhang et al., 2020).

1.3 Felsic veins from Holes U1473A and 735B

Several papers have been published focusing on the felsic veins drilled in the Atlantis Bank at the SWIR. By investigating seven felsic veins cutting through gabbro in Hole U1473A, Nguyen et al. (2018) determined that the formation occurred through fractional crystallization. Based on a structural geological survey of 14 felsic veins, Ma et al. (2020) discussed two generations of felsic veins in the core drilled in Hole U1473A. For type-1 veins, they proposed late fractional crystallization as the formation model. For type-2 veins, which are associated with dikes, the authors considered it to be the case that anatectic melts were formed by hydrous partial melting of gabbros, triggered by fluids derived from seawater. While the focus of this study is on structural geology, no valid geochemical or petrological evidence is presented for the mode of formation of the veins studied, except for some microstructures and An-rich rims in the plagioclases of the host gabbros, suggesting a genesis by hydrous partial melting of gabbro. Other authors investigating these veins focused on fractional crystallization as the relevant process, resulting from oxide fractionation at a late stage of tholeiitic magma evolution (Niu et al., 2002; Chen et al., 2019). For the felsic veins in Hole 735B, Chen et al. (2019) concluded that the formation of the felsic melts was primarily due to extreme fractional crystallization, as suggested by the bulk TiO_2 vs. MgO trend. However, this trend is highly heterogeneous and is based on only a few data points, which appear to have been affected by contamination from cumulate phases in the host gabbros. The most recent paper investigating the formation mode of felsic veins drilled in Hole U1473A is by Zhang et al. (2025), with a focus on the geochemistry of zircons and geochemical modeling. These authors provide compelling evidence that both extreme fractionation of MORB and hydrous partial melting of gabbros played significant roles in the formation of felsic melts at the Atlantis Bank.

Koepke et al. (2005a, b) focused on microstructures in gabbros from slow-spreading ridges and suggested that the felsic veins could be the result of partial melting triggered by high-temperature hydrothermal fluids that were transported along grain boundaries deep into the crust via high-temperature shear zones. In Koepke et al. (2005b), one example from the Atlantis Bank at the SWIR drilled in Hole 735B is presented. This model is also supported by the relatively low TiO_2 concentration in the veins, which is a consequence of the depleted nature of typical cumulate gabbros in the lower oceanic crust (see Koepke et al., 2007, for details). Finally, Natland et al. (1991) proposed liquid immiscibility between an oxide-rich and a silicate-rich melt as the possible origin of the felsic veins from Hole 735B. Pietranik et al. (2017) examined the composition of zircons in felsic veins and oxide gabbros from Hole 735B. Their findings suggest that there are different ways in which felsic melt can form. The zircons generally exhibit variable compositions, which is consistent with their crystallization from melts formed by crystal fractionation of mid-ocean ridge basalt (MORB) and hydrous partial remelting of deep cumulate gabbros.

1.4 Aims of this study

This study aims to provide evidence that hydrous partial melting of gabbros is one of the processes responsible for the formation of felsic veins in gabbros from Hole 735B. Until now, the microstructures of residual phases produced by hydrous partial-melting reactions have only been documented in a few locations in the recent oceanic crust generated at slow-spreading ridges (Koepke et al., 2005a, b). Of the Atlantis Bank at the SWIR, where the majority of studies on felsic veins cutting gabbros have been published, only one rock example has been presented by Koepke et al. (2005b) to date. This paper addresses the issue by presenting numerous additional examples of these characteristic microstructures in drilled gabbros from the Atlantis Bank at the SWIR.

Unlike the many studies on felsic veins from Hole 735B mentioned above, this paper focuses not on the petrology and geochemistry of the felsic veins themselves but on the microstructures preserved in the gabbros, which imply that hydrous partial melting has occurred. Key features of this process include zones of An-enriched plagioclase on grain boundaries, which form parageneses with interstitial brown amphibole and orthopyroxene. These can be interpreted as the residual phase assemblage left behind following a hydrous partial-melting event. The relevant microstructures have been found in about half of the gabbroic rocks from the ODP drill core 735B investigated in this study, emphasizing the importance of hydrous partial melting of gabbro as a mode of felsic melt formation. As these microstructures are often overlooked during petrographic work, this paper provides a catalogue of examples demonstrating how they can be identified using back-scattered electron (BSE) imaging alongside microanalytical tools (Figs. S1–S14 in the Supplement).

2 Materials and methods

2.1 Samples

In total, 29 gabbroic samples from drill core 735B have been investigated. Of these, 14 samples exhibited microstructures and compositions at grain boundaries that indicated the occurrence of hydrous partial-melting processes. For these 14 samples, electron microprobe data are presented (Table 1). Additionally, analytical profiles for each sample across grain boundaries between plagioclase grains affected by hydrous partial melting are presented, as well as back-scattered electron images (see the Supplement). A cathodoluminescence (CL) light image for one sample is also presented (Fig. 2).

https://doi.org/10.5194/ejm-38-179-2026

Table 1. Analyses of minerals of gabbros from ODP Hole 735B.

Sample[a]	Litho[b]	Min[c]	Qual.1[d]	Qual.2[e]	Am name[f]	C/r[g]	No.[h]	SiO_2	TiO_2	Al_2O_3	Cr_2O_3	FeO^{tot}	MnO	NiO	MgO	CaO	Na_2O	K_2O	Cl	Total	Mg#[i]	An#[j]	Temp[k]
90-1-61-67	ol gb	ol	pri			co	4	39.48	–	–		17.32	0.22	0.16	43.87	0.05	–	–		101.10	81.87		
								0.07				*0.17*	*0.14*	*0.02*	*0.08*								
90-1-61-67	ol gb	cpx	pri	pop1		co	2	52.48	0.62	2.80	0.22	5.38	0.23		18.33	20.32	0.33	–		100.71	85.86		
								0.11	*0.04*	*0.06*	*0.01*	*0.02*	*0.03*		*0.08*	*0.07*	*0.01*						
90-1-61-67	ol gb	cpx	pri	pop2		co	5	52.64	0.09	0.78	–	8.92	–		12.76	24.97	0.23	–		100.39	71.83		
								0.56	*0.11*	*0.80*		*2.19*			*1.31*	*0.32*	*0.17*						
90-1-61-67	ol gb	pl	pri			co	5	51.07		30.45		0.14			–	14.01	3.78	0.023		99.47		67.11	
								0.83		*0.29*		*0.05*				*0.60*	*0.37*	*0.01*					
90-1-61-67	ol gb	pl	HPM	repr				45.11		34.54					–	18.60	0.93	0.008		99.19		91.66	
90-1-61-67	ol gb	am	int		parg	co	4	46.58	1.22	10.71		5.82	0.09		18.34	12.45	2.58	0.14	–	97.95	84.88		717
								0.94	*0.13*	*0.92*		*0.23*	*0.01*		*0.50*	*0.04*	*0.17*	*0.01*					
121-1-14-19	ol gb	ol	pri			co	12	37.60	–	–		26.59	0.40		35.99	0.04	–	–		100.62	70.70		
								0.22				*0.39*	*0.04*		*0.45*	*0.03*							
121-1-14-19	ol gb	cpx	pri			co	23	51.27	0.88	2.70		7.19	0.24		15.56	20.89	0.41	–		99.15	79.42		
								0.24	*0.09*	*0.13*		*0.25*	*0.04*		*0.37*	*0.48*	*0.06*						
121-1-14-19	ol gb	opx	int			co	3	53.77	0.31	1.22		16.06	0.33		27.06	1.04	–	–		99.79	75.03		
								0.13	*0.02*	*0.03*		*0.36*	*0.02*		*0.17*	*0.06*							
121-1-14-19	ol gb	pl	pri			co	5	53.45	0.037	29.05		0.21	–		–	11.57	5.09	0.053		99.46		55.50	
								0.32	*0.01*	*0.29*		*0.05*				*0.17*	*0.10*	*0.01*					
121-1-14-19	ol gb	pl	HPM	repr				48.58	–	32.35		0.33			0.031	15.70	2.63	0.021		99.64		76.63	
121-1-14-19	ol gb	am	int		Ti parg	co	15	42.94	3.21	11.69		9.68	0.11		15.05	11.38	2.54	0.19		96.79	73.50		961
								0.34	*0.47*	*0.20*		*0.29*	*0.04*		*0.48*	*0.15*	*0.18*	*0.02*					
137-6-112-119	ol gb	ol	pri			co	8	35.58	–	–	–	36.91	0.66	–	26.73	0.07	–	–		99.95	56.35		
								0.35				*0.64*	*0.03*		*0.33*	*0.06*							
137-6-112-119	ol gb	cpx	pri			co	12	50.97	0.73	2.43	–	9.82	0.30		13.98	20.41	0.42	–		99.06	71.74		
								0.18	*0.06*	*0.08*		*0.42*	*0.04*		*0.27*	*0.62*	*0.02*						
137-6-112-119	ol gb	opx	int			co	9	53.00	0.18	0.97	–	21.11	0.52		22.97	0.90	–	–		99.65	65.98		
								0.21	*0.03*	*0.04*		*0.26*	*0.06*		*0.17*	*0.13*							
137-6-112-119	ol gb	pl	pri			co	7	54.88	–	28.80		0.35	–		–	10.95	5.36	0.060		100.40		52.85	
								0.47		*0.40*		*0.07*				*0.39*	*0.27*	*0.02*					
137-6-112-119	ol gb	pl	HPM	repr				48.92	–	32.27		0.50			–	15.56	2.76	0.020		100.03		75.58	
137-6-112-119	ol gb	am	int		parg	co	11	42.65	2.62	11.32	–	12.62	0.17		13.20	11.16	2.64	0.31	–	96.69	65.09		907
								0.68	*0.52*	*0.29*		*0.35*	*0.03*		*0.40*	*0.22*	*0.16*	*0.02*					
142-1-114-120	ol gb	ol	pri			co	10	36.81	–	–	–	30.52	0.49	0.07	32.77	0.05	–	–		100.72	65.69		
								0.32				*0.31*	*0.07*	*0.03*	*0.28*	*0.02*							
142-1-114-120	ol gb	cpx	pri			co	12	51.34	0.68	2.81	0.09	7.54	0.18		16.59	20.15	0.38	–		99.75	79.68		
								0.40	*0.10*	*0.08*	*0.05*	*0.64*	*0.05*		*0.30*	*0.28*	*0.03*						

Table 1. Continued.

Sample[a]	Litho[b]	Min[c]	Qual.1[d]	Qual.2[e]	Am name[f]	C/r[g]	No.[h]	SiO_2	TiO_2	Al_2O_3	Cr_2O_3	FeO^{tot}	MnO	NiO	MgO	CaO	Na_2O	K_2O	Cl	Total	Mg#[i]	An#[j]	Temp[k]
142-1-114-120	ol gb	opx	int			co	10	53.07	0.32	1.05	–	18.78	0.45		25.15	1.21	0.03	–		100.06	70.48		
								0.29	*0.01*	*0.15*		*0.37*	*0.08*		*0.21*	*0.18*	*0.02*						
142-1-114-120	ol gb	pl	pri			co	35	54.46	0.024	28.79		0.30			0.008	11.33	5.30	0.051		100.27		54.01	
								0.36	*0.01*	*0.26*		*0.08*			*0.01*	*0.28*	*0.18*	*0.02*					
142-1-114-120	ol gb	pl	HPM	repr				45.37	0.012	34.37		0.15			–	18.44	1.31	0.005		99.66		88.56	
142-1-114-120	ol gb	am	int	pop1	Ti mg hast	co	5	42.03	4.17	10.73	0.06	11.56	0.15	–	13.92	11.46	2.61	0.26	0.008	96.95	68.22		1017
								0.30	*0.07*	*0.08*	*0.01*	*0.13*	*0.02*		*0.25*	*0.07*	*0.04*	*0.02*	*0.00*				
142-1-114-120	ol gb	am	int	pop2	Ti parg	co	6	42.53	3.43	11.63	0.05	11.25	0.14	–	13.98	11.87	2.37	0.27	0.013	97.52	68.90		978
								0.23	*0.03*	*0.12*	*0.01*	*0.23*	*0.03*		*0.10*	*0.15*	*0.05*	*0.01*	*0.02*				
144-5-108-113	ol gb	ol	pri			co	9	36.83	–	–		30.73	0.47		32.96	0.06	–	–		101.05	65.66		
								0.19				*0.33*	*0.06*		*0.27*	*0.02*							
144-5-108-113	ol gb	ol	pri			ri	9	36.97	–	–		30.55	0.49		32.98	0.03	–	–		101.03	65.81		
								0.20				*0.56*	*0.04*		*0.45*	*0.02*							
144-5-108-113	ol gb	cpx	pri			co	15	51.33	0.60	2.77		6.74	0.18		16.27	20.87	0.40	–		99.16	81.13		
								0.70	*0.16*	*0.30*		*0.98*	*0.05*		*1.00*	*0.66*	*0.09*						
144-5-108-113	ol gb	pl	pri			co	9	52.82	0.053	29.86		0.19	–		–	12.03	4.79	0.048		99.80		57.95	
								0.76	*0.02*	*0.54*		*0.05*				*0.49*	*0.24*	*0.02*					
144-5-108-113	ol gb	pl	HPM	repr				49.34	0.010	32.11		0.20			–	14.90	3.17	0.018		99.76		72.12	
144-5-108-113	ol gb	am	int		mg hast	co	10	42.54	1.53	12.21		11.79	0.17		14.71	10.76	2.81	0.22		96.73	68.99		766
								0.76	*0.26*	*0.84*		*0.63*	*0.03*		*0.48*	*0.20*	*0.15*	*0.02*					
149-2-61-65	ol gb	pl	pri			co	10	55.24	0.036	28.50		0.25	–		–	10.91	5.46	0.067		100.47		52.26	
								0.30	*0.01*	*0.16*		*0.01*				*0.15*	*0.16*	*0.00*					
149-2-61-65	ol gb	pl	HPM	repr				47.14	–	33.69		0.52			–	17.39	1.85	0.022		100.61		83.71	
149-3-53-61	dis ox gb	ol	pri			co	9	36.01	–	–	–	34.38	0.48	–	29.86	0.06	–	–		100.79	60.76		
								0.14				*0.51*	*0.05*		*0.19*	*0.03*							
149-3-53-61	dis ox gb	opx	int			co	9	53.52	0.14	0.92	–	20.12	0.48		24.73	0.93	–	–		100.84	68.66		
								0.24	*0.01*	*0.06*		*0.26*	*0.04*		*0.27*	*0.10*							
149-3-53-61	dis ox gb	pl	pri			co	22	55.61	0.020	28.02		0.38			–	10.44	5.70	0.097		100.28		50.01	
								0.63	*0.01*	*0.38*		*0.18*				*0.34*	*0.25*	*0.01*					
149-3-53-61	dis ox gb	pl	HPM	repr				48.74	–	32.88		0.64				15.88	2.53	0.032		100.71		77.50	
149-3-53-61	dis ox gb	am	int		Ti parg	co	1	42.58	2.93	11.68	–	11.99	0.14	–	13.80	11.40	2.90	0.36	0.007	97.79	67.23		937
149-3-76-80	ol gb	ol	pri			co	4	36.45	–	–		33.69	0.55	–	29.81	–	–	–		100.50	61.20		
								0.09				*0.38*	*0.08*		*0.36*								
149-3-76-80	ol gb	cpx	pri			co	6	52.41	0.39	1.49	–	8.66	0.23		14.64	21.90	0.39	–		100.12	75.09		
								0.29	*0.07*	*0.10*		*0.38*	*0.07*		*0.09*	*0.46*	*0.02*						
149-3-76-80	ol gb	opx	pri			co	3	53.06	0.34	0.96	–	20.26	0.54		23.63	1.52	–	–		100.31	67.53		
								0.14	*0.04*	*0.10*		*0.34*	*0.03*		*0.18*	*0.17*							

https://doi.org/10.5194/ejm-38-179-2026

Table 1. Continued.

Sample[a]	Litho[b]	Min[c]	Qual.1[d]	Qual.2[e]	Am name[f]	C/r[g]	No.[h]	SiO_2	TiO_2	Al_2O_3	Cr_2O_3	FeO^{tot}	MnO	NiO	MgO	CaO	Na_2O	K_2O	Cl	Total	Mg#[i]	An#[j]	Temp[k]
149-3-76-80	ol gb	opx	incl			co	3	53.38	0.25	0.71	–	20.85	0.57		23.48	1.13	–	–		100.37	66.75		
								0.21	*0.06*	*0.09*		*0.19*	*0.03*		*0.13*	*0.17*							
149-3-76-80	ol gb	pl	pri			co	6	55.26		27.67		0.39			–	10.64	5.66	0.110		99.73		50.63	
								0.46		*0.33*		*0.12*				*0.22*	*0.25*	*0.01*					
149-3-76-80	ol gb	pl	HPM	repr				48.47		32.16		0.42				16.14	2.46	0.029		99.67		78.28	
149-3-76-80	ol gb	am	int		parg	co	6	42.53	2.15	11.99		11.95	0.15		14.05	11.25	2.78	0.36	–	97.21	67.70		853
								0.17	*0.06*	*0.25*		*0.26*	*0.01*		*0.18*	*0.14*	*0.06*	*0.05*					
157-4-1-9	ol gb	ol	pri			co	5	36.54	–	–	–	33.39	0.53	–	30.00	0.02	–	–		100.48	61.56		
								0.16				*0.54*	*0.07*		*0.37*	*0.02*							
157-4-1-9	ol gb	cpx	pri			co	10	51.04	0.69	2.36		8.95	0.30		13.73	21.26	0.49	–		98.82	73.21		
								0.36	*0.10*	*0.33*		*0.33*	*0.03*		*0.13*	*0.60*	*0.15*						
157-4-1-9	ol gb	opx	int			co	16	53.17	0.08	1.32	–	20.20	0.58		24.12	0.63	–	–		100.10	68.04		
								0.26	*0.05*	*0.15*		*0.60*	*0.07*		*0.45*	*0.14*							
157-4-1-9	ol gb	pl	pri			co	11	55.60	–	27.72		0.22	–		–	10.21	5.77	0.030		99.55		49.35	
								0.54		*0.37*		*0.06*				*0.33*	*0.11*	*0.02*					
157-4-1-9	ol gb	pl	HPM	repr				49.24	–	31.82		0.26			–	15.00	2.90	0.021		99.24		73.99	
157-4-1-9	ol gb	am	int	pop 1	mg hast	co	14	42.02	1.67	13.66	–	11.91	0.21	–	14.28	10.61	2.63	0.29	–	97.28	68.12		788
								0.19	*0.10*	*0.35*		*0.28*	*0.02*		*0.18*	*0.31*	*0.10*	*0.04*					
157-4-1-9	ol gb	am	int	pop 2	mg hast	co	10	42.63	1.20	12.83	–	12.20	0.22	–	14.16	11.12	2.41	0.31	–	97.08	67.42		714
								0.23	*0.41*	*0.53*		*0.31*	*0.05*		*0.25*	*0.20*	*0.12*	*0.01*					
170-7-50-55	ol gb	ol	pri			co	5	37.57	–	–		26.56	0.39	0.05	34.49	0.02	–	–		99.09	69.83		
								0.19				*0.19*	*0.07*	*0.06*	*0.23*	*0.01*							
170-7-50-55	ol gb	cpx	pri			co	5	51.14	0.98	2.83	0.25	7.30	0.19		14.99	20.83	0.48	–		98.98	78.55		
								0.70	*0.11*	*0.77*	*0.24*	*1.23*	*0.05*		*0.60*	*1.48*	*0.13*						
170-7-50-55	ol gb	pl	pri			co	4	54.38	0.070	28.98		0.17			–	11.40	4.92	0.058		99.98		55.96	
								0.21	*0.01*	*0.09*		*0.04*				*0.09*	*0.10*	*0.00*					
170-7-50-55	ol gb	pl	HPM	repr				49.86	–	31.08		0.18			–	14.72	3.19	0.018		99.05		71.75	
170-7-50-55	ol gb	am	int		parg	co	1	44.92	1.01	11.12		9.29	0.16		15.63	11.68	2.13	0.24		96.17	75.00		680
176-6-132-138	ol gb	ol	pri			co	38	37.90	–	–		26.10	0.40	0.08	36.24	0.04	–	–		100.77	71.22		
								0.28				*0.29*	*0.04*	*0.04*	*0.42*	*0.03*							
176-6-132-138	ol gb	cpx	pri			co	39	51.77	0.87	2.59	0.19	7.35	0.22		15.51	21.30	0.42	–		100.20	79.01		
								0.37	*0.16*	*0.24*	*0.04*	*0.64*	*0.03*		*0.48*	*0.92*	*0.05*						
176-6-132-138	ol gb	opx	int			co	58	54.40	0.21	1.13	–	15.86	0.37		27.09	0.84	–	–		99.90	75.28		
								0.57	*0.11*	*0.22*		*0.26*	*0.06*		*0.44*	*0.22*							

Table 1. Continued.

Sample[a]	Litho[b]	Min[c]	Qual.1[d]	Qual.2[e]	Am name[f]	C/r[g]	No.[h]	SiO_2	TiO_2	Al_2O_3	Cr_2O_3	FeO^{tot}	MnO	NiO	MgO	CaO	Na_2O	K_2O	Cl	Total	Mg#[i]	An#[j]	Temp[k]
176-6-132-138	ol gb	pl	pri			co	63	54.29	0.054	28.88		0.20			–	11.41	5.15	0.051		100.03		54.86	
								0.33	*0.02*	*0.20*		*0.05*				*0.20*	*0.12*	*0.01*					
176-6-132-138	ol gb	pl	HPM	repr				48.76	0.010	31.73		0.20			0.006	15.49	2.87	0.028		99.09		74.78	
176-6-132-138	ol gb	am	int		parg	co	33	43.37	2.57	11.65	0.21	9.75	0.12		15.13	11.78	2.50	0.21		97.29	73.45		903
								0.48	*0.45*	*0.34*	*0.11*	*0.26*	*0.04*		*0.41*	*0.18*	*0.15*	*0.03*					
202-8-7-16	ol gb	ol	pri			co	5	37.34	–	–		28.68	0.50	0.07	32.76	0.05	–	–		99.39	67.1		
								0.19				*0.22*	*0.05*	*0.02*	*0.33*	*0.02*							
202-8-7-16	ol gb	cpx	pri			co	4	50.77	0.97	3.03	0.20	8.73	0.31		14.41	20.33	0.41	–		99.16	74.6		
								0.44	*0.16*	*0.17*	*0.03*	*1.22*	*0.03*		*0.59*	*1.69*	*0.03*						
202-8-7-16	ol gb	pl	pri			co	5	53.23	0.038	29.32		0.25			–	11.97	4.51	0.067		99.38		59.22	
								0.52	*0.01*	*0.20*		*0.04*				*0.29*	*0.09*	*0.01*					
202-8-7-16	ol gb	pl	HPM	repr				50.29	–	30.76		0.24			0.017	14.56	3.28	0.045		99.18		70.89	
202-8-7-16	ol gb	am	int		Ti parg	co	6	42.65	2.93	11.58	0.16	10.56	0.13		14.02	11.65	2.43	0.29		96.40	70.31		938
								0.33	*0.43*	*0.19*	*0.07*	*0.40*	*0.04*		*0.23*	*0.10*	*0.13*	*0.02*					
206-2-46-52	ol gb	ol	pri			co	8	38.23	–	–	–	23.51	0.31	–	37.98	0.02	–	–		100.05	74.23		
								0.11				*0.41*	*0.04*		*0.33*	*0.01*							
206-2-46-52	ol gb	cpx	pri			co	10	51.85	0.64	2.67	0.07	7.44	0.21		16.10	20.44	0.36	–		99.77	79.40		
								0.25	*0.02*	*0.10*	*0.03*	*0.92*	*0.02*		*0.99*	*1.72*	*0.04*						
206-2-46-52	ol gb	opx	int			co	11	54.42	0.26	1.21	–	14.73	0.37		28.03	0.91	–	–		99.93	77.23		
								0.11	*0.06*	*0.05*		*0.30*	*0.05*		*0.30*	*0.25*							
206-2-46-52	ol gb	pl	pri			co	6	53.10	0.080	29.19		0.26	–		–	12.04	4.60	–		99.27		59.12	
								0.68	*0.03*	*0.43*		*0.06*				*0.54*	*0.59*						
206-2-46-52	ol gb	pl	HPM	repr				47.56		32.90		0.36				16.52	2.20	0.026		99.57		80.46	
206-2-46-52	ol gb	am	int		parg	co	14	43.46	2.55	11.62	–	9.61	0.13	–	15.11	11.82	2.09	0.26	–	96.65	73.71		900
								0.13	*0.07*	*0.10*		*0.16*	*0.02*		*0.18*	*0.17*	*0.06*	*0.02*					
207-4-64-70	ol gb	ol	pri			co	10	38.35	–	–	–	22.37	0.33	0.04	38.82	0.02	–	–		99.93	75.57		
								0.51				*0.42*	*0.06*	*0.07*	*0.48*	*0.02*							
207-4-64-70	ol gb	cpx	pri			co	8	51.66	0.70	2.43	–	6.49	0.18		16.02	21.98	0.39	–		99.84	81.48		
								0.44	*0.03*	*0.06*		*0.31*	*0.04*		*0.48*	*0.65*	*0.05*						
207-4-64-70	ol gb	opx	int			co	9	54.30	0.23	1.27	–	14.33	0.32		28.67	0.82	–	–		99.94	78.10		
								0.37	*0.06*	*0.08*		*0.53*	*0.04*		*0.44*	*0.08*							
207-4-64-70	ol gb	pl	pri			co	8	52.60	0.040	29.71		0.28	–		–	12.47	4.70	0.040		99.84		59.32	
								0.61	*0.03*	*0.17*		*0.04*				*0.26*	*0.18*	*0.01*					
207-4-64-70	ol gb	pl	HPM	repr				49.50	–	31.54		0.27			–	15.46	3.06	0.021		99.84		73.53	
207-4-64-70	ol gb	am	int		mg hast	co	2	43.80	2.05	11.80	0.07	9.17	0.06	–	16.05	12.22	2.21	0.16	–	97.58	75.74		841
								0.29	*0.00*	*0.40*	*0.02*	*0.30*	*0.06*		*0.22*	*0.01*	*0.04*	*0.01*					

[a] Sample description according to IODP code: core – section – from (cm) – to (cm); all from ODP Hole 735B. [b] Ol gb – olivine gabbro; diss ox gb – disseminated oxide olivine gabbro. [c] Mineral: ol – olivine; cpx – clinopyroxene; opx – orthopyroxene; pl – plagioclase; am – amphibole. [d] Qualifier 1: HPM – An-enriched plagioclase formed by hydrous partial melting; incl – inclusion; pri – primary; int – interstitial. [e] Qualifier 2: pop – population; repr – representative analysis. [f] Amphibole name: mg hast – magnesiohastingsite; parg – pargasite; Ti mg hast – Ti-rich magnesio-hastingsite; Ti parg – Ti-rich pargasite; according to Locock (2014). [g] Core/rim analysis. [h] Number of analyses. [i] $MgO/(MgO + FeO^{tot}) \cdot 100$, molar. [j] An content of the plagioclase, mol %. [k] Equilibrium temperature according to the Ti-in-amphibole geothermometer of Ernst and Liu (1998). The en dash (–) means below limit of detection (see text for details). Empty space: not analyzed. Rows in italics: one standard deviation.

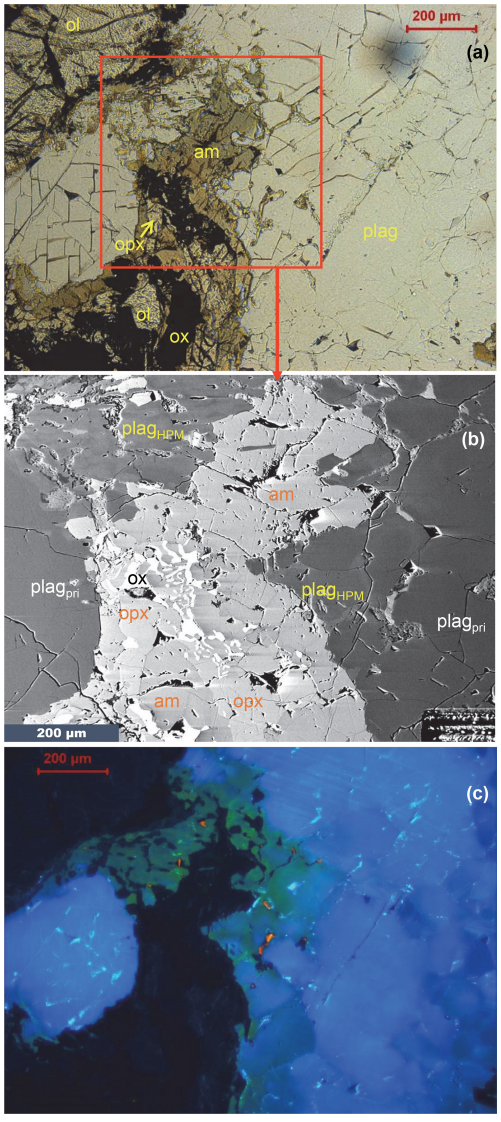

Figure 2. Different types of micrographs from the same location in olivine gabbro 157-4-1-9, which has been strongly influenced by the effects of hydrous partial melting. **(a)** Microscope image with plane-polarized light. In the center, there is a domain that has been strongly influenced by hydrous partial melting. This consists of the residual phases amphibole (am) and orthopyroxene (opx). An-enriched plagioclase, which is also present in this domain, cannot be distinguished from primary plagioclase grains (plag). The primary phases visible besides plagioclase are olivine (ol) and Fe–Ti oxides (ox). **(b)** BSE image showing a zoom-in from **(a)**, focusing on the central domain. Zones of An-enriched plagioclase on grain boundaries of the primary plagioclases are now visible. These zones are characterized by slightly lighter-gray levels due to their higher An content ($plag_{HPM}$ with HPM: hydrous partial melting), while primary plagioclase shows a darker-gray level ($plag_{pri}$). **(c)** The CL image shows that zones with a high An content in plagioclase, as a result of a hydrous partial-melting reaction, are yellow in color. In contrast, primary plagioclase grains unaffected by this reaction are blue. Mafic silicates and Fe–Ti oxides appear to be black. The tiny red dots correspond to apatite. For details, see the text.

2.2 Methods

Mineral phases were analyzed using an electron microprobe. Around 5000 analyses, primarily via profiles through grain boundaries affected by hydrous partial melting, have been presented. Of these, 79 averages were evaluated based on approximately 800 individual analyses. The data are shown in Table 1.

A Cameca SX100 electron microprobe, equipped with five spectrometers and operating with the Cameca software "Peak Sight", was used. All data were obtained using a static (fixed) beam, Kα emission from all elements, and a 15 kV acceleration potential. The "PAP" matrix correction (Pouchou and Pichoir, 1991) was applied using natural and synthetic standards. Most element concentrations were obtained with a beam current of 15 nA and a counting time of 10 s for the peak and background. Higher beam currents (40 nA) and increased counting times (60–120 s) were applied for F and Cl in amphibole and for Mg, Ti, and K in plagioclase, leading to more accurate trace element data and lower limits of detection. The limits of detection (in wt %) are as follows: TiO_2 in mafic silicates – 0.03; TiO_2 in plagioclase – 0.01; Al_2O_3 in mafic silicates – 0.02; Cr_2O_3 and NiO in silicates – 0.04; MnO in mafic silicates – 0.03; MgO in plagioclase – 0.005; CaO in olivine – 0.02; Na_2O and K_2O in mafic silicates – 0.02; K_2O in plagioclase – 0.005; Cl in brown amphibole – 0.005; F in brown amphiboles amphibole – 0.1. As the F content of brown amphibole is mostly below the detection limit and because the data are highly scattered, the F content of amphiboles has not been considered and has been excluded from the data table.

3 Results

3.1 Petrography

The gabbroic rocks investigated in Hole 735B are oxide-bearing olivine gabbros. They exhibit a granular texture ranging from fine to coarse, and foliation is sometimes visible due to crystal–plastic deformation. This phenomenon is evident in numerous gabbros from this site (e.g., Dick et al., 2000). The rocks consist of primary plagioclase, clinopyroxene, and olivine and often contain prismatic orthopyroxene. There is frequently a notable secondary mineral growth consisting of brown amphibole, orthopyroxene, and Fe–Ti oxides, which rim the primary minerals and form granular interstitial assemblages.

The focus of this paper is these interstitial assemblages. They are usually explained by typical late-stage crystallization, precipitated from the final melt drops enriched in SiO_2 and incompatible elements such as P and Zr. This enables the crystallization of apatite and zircon, respectively (see Koepke et al., 2018, for details). However, if such late-stage paragenesis also contains zones of plagioclase that are strongly enriched in An content, it is much more probable that the miner-

als form a residual assemblage after hydrous partial melting of the gabbro (Koepke et al., 2005a, b; Wolff et al., 2013). This is demonstrated in Fig. 2, which shows such an assemblage. Microscope images taken using plan-polarized or cross-polarized light do not reveal the zones of An-enriched plagioclases. It is not possible to distinguish between the two modes of forming interstitial parageneses in such an image (Fig. 2a). However, a solution is provided by BSE images, in which the An-enriched plagioclases can be easily identified. These normally nucleate at the grain boundary between grains of primary plagioclase. Due to their higher density and, consequently, greater electron backscattering effect, these zones appear to be brighter in BSE images, enabling them to be distinguished from the darker host plagioclase (Fig. 2b). BSE images of these parageneses in the samples investigated, which are indicative of proceeded hydrous partial melting of gabbro, are presented in the Supplement.

Another way to identify zones containing An-enriched plagioclase is to use CL light. Exposing the sample surface to electrons results in photon emissions that produce luminescence in the mineral phases, which has a characteristic color corresponding to the luminescence wavelength. This is a complex function of trace element substitutions and defect structures in the irradiated minerals. As the An-rich plagioclase produced by partial melting exhibits a notably distinct trace element composition (see Sect. 3.2), the reactive plagioclase at grain boundaries exhibits a notably different luminescence color (yellow-green color in Fig. 2c), contrasting with the primary plagioclase with lower An content (blue in Fig. 2c).

3.2 Mineral compositions

The mineral analyses obtained using (electron probe microanalysis) EPMA are presented in Table 1. The primary minerals are highly homogeneous, with no significant zoning. The Mg# (molar $MgO/(MgO + FeO) \cdot 100$) of olivine and the An content of primary plagioclase are relatively low, ranging from 56 to 82 and from 49 to 67 mol %, respectively. This is because the gabbros from the Atlantis Bank at the SWIR are relatively evolved (see Coogan, 2014; Dick et al., 2000, 2002), as can be seen in the Mg# in olivine versus the An content in plagioclase diagram (Fig. 3). This diagram shows the magmatic evolution of the gabbros investigated, which follows the same trend as the whole 735B drill core (Dick et al., 2002).

As mentioned above, the focus of this paper is on the secondary interstitial minerals generated by the hydrous partial melting of gabbros. This is indicated by zones of An-enriched plagioclase at the boundaries between primary plagioclase grains, which coexist with interstitial brown amphibole and orthopyroxene. To verify the An enrichment in the plagioclase, BSE imaging and EPMA profiling through such zones at plagioclase–plagioclase grain boundaries have been performed. This is demonstrated by an example, showing a typical interstitial paragenesis consisting of brown amphibole, orthopyroxene, and An-enriched plagioclase, which are embedded within the primary granular cumulate assemblage of olivine, clinopyroxene, and plagioclase lower in An (Fig. 4). The plagioclase compositions in such zones exhibit distinctive characteristics. Aside from the substantial enrichment in An content, they are significantly depleted in trace elements, as illustrated in Fig. 4 for the elements Mg, Ti, and K. The corresponding analyses with EPMA have been performed by applying significantly higher beam currents and counting times, resulting in more accurate trace element data and lower limits of detection (for details see Sect. 2.2). A further characteristic feature of such zones is the asymmetrical, heterogeneous nature of the compositional profiles (Fig. 4), which is the reason why it is not possible to present simple average values of the An-enriched plagioclase. Representative analyses of plagioclase with the strongest An enrichment in such zones are presented in Table 1 instead.

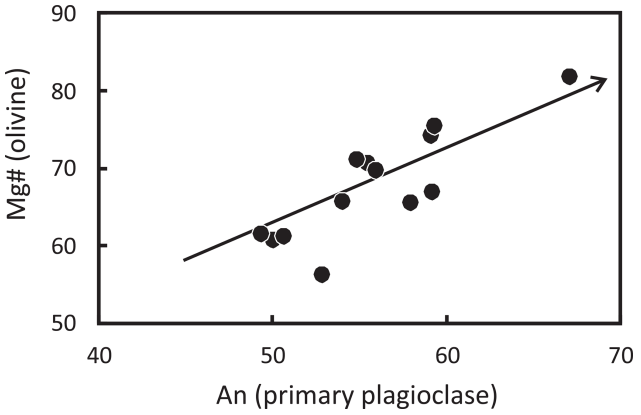

Figure 3. Mg# of olivine versus the An content of primary plagioclases in the investigated samples. The arrow indicates the general trend of evolution for gabbros based on data from Dick et al. (2002) from drill core 735B.

Mg# of orthopyroxene varies between 66 and 78, which is significantly higher than values for the corresponding primary olivines of the same rock, varying between 56 and 76 (Table 1). Brown amphibole forming rim and interstitial parageneses with orthopyroxene and An-enriched plagioclase are of pargasitic/hastingsitic composition, with high concentrations of Na_2O (from 2.1 to 2.9 wt %) and Al_2O_3 (from 10.7 to 13.7 wt %, Table 1). The TiO_2 contents are relatively high, leading to formation temperatures by applying the Ti-in-amphibole geothermometer of Ernst and Liu (1998) from 717 to 1017 °C (Table 1), mostly indicating a magmatic formation overlapping with the magmatic–metamorphic regime. Volatile contents are generally low, with F contents mostly below the EPMA detection limit and a Cl content varying from below the detection limit to 0.01 wt %.

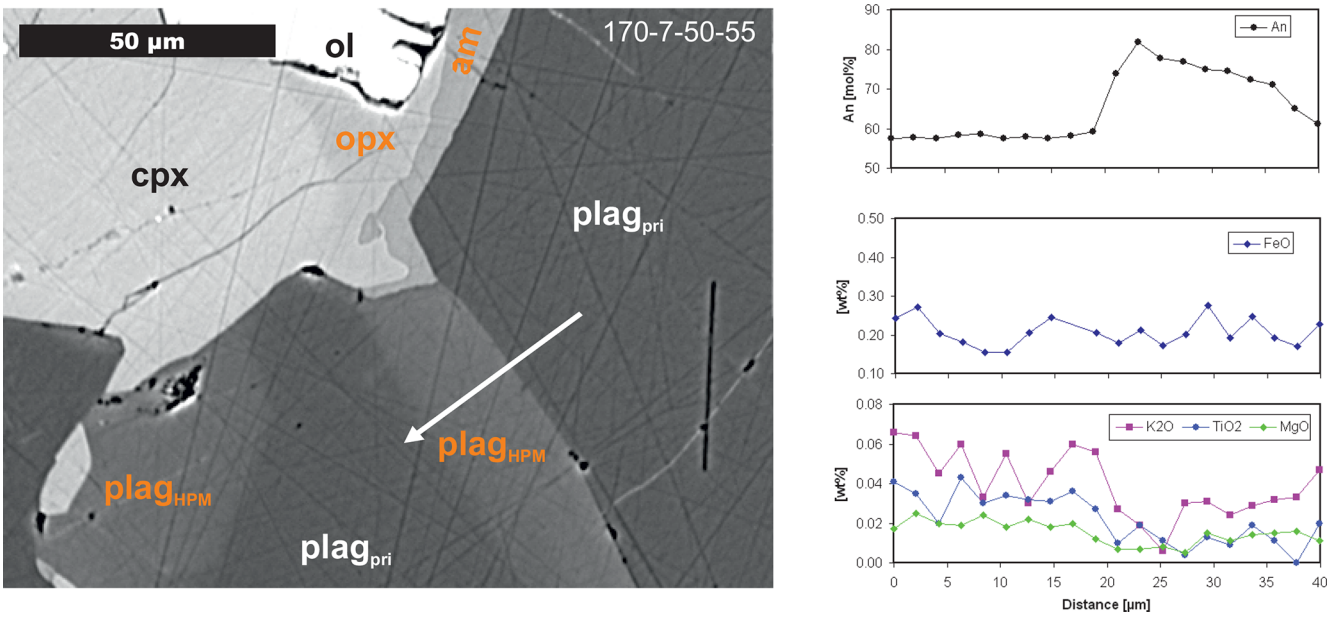

Figure 4. Left: BSE image showing a typical residual phase assemblage in an olivine gabbro (sample 170-7-50-55), generated by partial melting triggered by water-rich fluids migrating along grain boundaries above the wet gabbro solidus. The primary phases that formed during crystallization and accumulation in an axial magma chamber beneath the ridge are olivine (ol), clinopyroxene (cpx), and plagioclase ($plag_{pri}$). After cooling of the cumulate network but still above the wet gabbro solidus, hydrous fluids migrated along grain boundaries, initiating partial melting. As a consequence of the incongruent partial-melting reaction, residual phases (named in orange) are formed: zones of plagioclase that are strongly enriched in An content are found along the grain boundaries of plagioclase ($plag_{HPM}$), as well as interstitial growth of amphibole (am) and orthopyroxene (opx) at the contact between these zones and the primary mafic minerals. Right: an EPMA profile showing the distribution of different elements across a zone of An-enriched plagioclase (marked by an arrow in the BSE image).

4 Discussion

4.1 Characteristic features of residual assemblages formed by hydrous partial melting of gabbro

Since gabbroic rocks from the Atlantis Bank are well known for their intense late-stage crystallization during magmatic processes, resulting in widespread occurrence of amphibole-bearing oxide gabbros (e.g., Dick et al., 2000, 2002; MacLeod et al., 2017), clear evidence is needed to confirm the formation of a similar interstitial assemblage as residual paragenesis following hydrous partial melting of gabbro. This will be discussed in more detail below, presenting all of the characteristic features that are indicative of a residual phase assemblage generated by the hydrous partial melting of gabbro.

1. The most striking feature is the presence of zones enriched in An at the grain boundaries between the primary plagioclases, which form parageneses with brown amphibole and orthopyroxene (Fig. 4). The reason for the An-enrichment in plagioclase is the transition from a dry system during cumulate formation to a system with high water activities during the partial-melting event. This causes plagioclase to crystallize with a high An content (e.g., Sisson and Grove, 1993; Berndt et al., 2005). This feature has also been reproduced in experimental studies of partial melting of gabbro (Koepke et al., 2004; Wolff et al., 2013). In an experimental study using "microrocks" as starting material, Wolff et al. (2013) managed to replicate the interstitial nature of the residual paragenesis following a partial-melting process. The authors highlighted the discontinuous nature of the partial-melting reaction, as evidenced by the interstitial growth of amphibole and orthopyroxene associated with primary olivine and clinopyroxene, as well as the growth of An-enriched plagioclase zones on grain boundaries between primary plagioclase grains. As presented in Fig. 5, the difference in An content between the An-enriched zones and the primary plagioclases in the investigated gabbros varies considerably, from 12 to 35 mol %. The zoning of the plagioclase, as indicated by the presence of An-rich rims, contrasts sharply with the typical zoning observed in many oceanic gabbros, including those from the Atlantis Bank. An example of normal zoning in plagioclases is presented in Fig. 6 for an olivine gabbro from the 735B drill core. As expected, an EPMA profile through a rim of such a normal-zoned plagioclase shows that it is impoverished in An content (Fig. 6). This is a consequence of the composition of typical late-stage melts, which are relatively evolved

compared to the primitive nature of MORB that fed the gabbro's main stage crystallization (e.g., Koepke et al., 2018). The presence of zones of An-enriched plagioclase on grain boundaries in oceanic gabbros is essential for a hydrous partial-melting formation model. The corresponding microstructures found in the 735B gabbros investigated, including EPMA traverses through zones of An-enriched plagioclase, are presented in the Supplement.

2. As shown in Fig. 4 and in the Supplement, trace elements such as Mg, Ti, and K are characteristically depleted in the plagioclase of the An-enriched zones. This is due to the formation processes involving high-temperature water-rich fluids impoverished in trace elements percolating on grain boundaries above the solidus temperature in wet gabbros (for details on the process, see Koepke et al., 2007, 2014; Wolff et al., 2013). Considering the solidus temperature of 800 °C for wet oxide gabbro (Koepke et al., 2018) and the estimated amphibole formation temperatures using the Ti-in-amphibole thermometer (Table 1), it is clear that conditions for hydrous partial melting were met. However, since trace elements are present in extremely low concentrations in such water-rich fluids, the residual plagioclase left after partial melting is very depleted in trace elements such as Mg, Ti, and K (Fig. 4). This contrasts with the composition of rims in normal-zoned plagioclase, formed by a late-evolved melt. In this case, these elements are enriched rather than depleted, as shown in Fig. 6 for K and Ti.

3. As shown in the experimental study of Koepke et al. (2018), minerals that crystallize interstitially in a late-magmatic stage should be more evolved than the crystals of the main-stage crystallization. The same should apply to orthopyroxene that crystallized interstitially in a late magmatic stage. However, the orthopyroxenes identified as residual phases following hydrous partial melting in the samples investigated, which coexist with An-rich plagioclase and brown amphibole, are more primitive than the main mafic phases (see Results; Table 1).

In summary, the three observations listed above strongly suggest that the observed microstructures formed through hydrous partial melting of gabbro rather than normal fractional crystallization at a later stage. Another compelling argument is that relating to the low bulk rock concentration of TiO_2 in the felsic veins, which is characteristic of the depleted nature of the cumulate gabbros starting material. Figure 7 shows the corresponding TiO_2 vs. SiO_2 diagram, including all published bulk data of felsic veins from the Atlantis Bank drill cores. The vast majority of the data points lie below the line representing the minimum TiO_2 values obtained from experiments on MORB differentiation in tholeiitic systems. This implies that at least some of the felsic veins in the Atlantis Bank drill core are formed by hydrous partial melting of gabbro. For this diagram to be applicable, the felsic veins must represent frozen melt and not cumulate rocks, as the surrounding gabbros do. Many of the felsic veins exhibit granophyric textures, consisting of intergrowths of quartz and albite-rich plagioclase (see MacLeod et al., 2017). This texture is believed to result from eutectic crystallization (e.g., Johannes and Holtz, 1996), which provides compelling evidence that the felsic veins formed from a melt. In summary, the results of this study independently support Zhang et al.'s (2025) conclusion that hydrous partial melting occurred in the gabbros of the Atlantis Bank, producing anatectic melts.

4.2 The source of water-rich fluids triggering partial melting: hydrothermal or magmatic?

In light of our finding that the drilled gabbros from Hole 735B underwent hydrous partial melting, the question arises as to whether the water-rich fluids were magmatic or hydrothermal. In general, only a very small amount of water is needed to produce water-saturated melts at low pressures. For example, at 1 kbar (equivalent to a depth of 3 km), around 2.5 wt % of water is needed to create a water-saturated melt (Berndt et al., 2002). While this corresponds to 100 % melt, the amount of melt is significantly lower during anatectic processes at ridges (see the experiments of Koepke et al., 2004). Thus, at this pressure, only a few droplets of water are enough to trigger partial melting. It is interesting to consider the water/rock ratio, which, in this case, is ~ 0.025 (to generate 100 % melt). In real conditions of hydrous partial melting under mid-ocean ridges, the water-to-rock ratio can be even lower. This implies that only a small amount of water at temperatures just above the gabbro solidus is necessary to initiate the partial-melting process in the gabbro. A key question is whether these water-rich fluids are of magmatic or hydrothermal origin. The usual approaches to answering this question are (1) applying stable isotopes to the felsic veins and (2) analyzing chlorine and fluorine in the magmatic phases in the related rocks, especially in amphibole and apatite. We will focus on these two aspects below.

1. Relatively high $^{87}Sr/^{86}Sr$ ratios and depleted $\delta^{18}O$ values in bulk rocks from the lower oceanic crust typically indicate that seawater is the most likely source of a water-rich fluid operating at a very high temperature in the deep oceanic crust (e.g., Bosch et al., 2004). However, if the water/rock ratios are very low (e.g., <0.025, as discussed above for the case of initial hydrous partial melting of gabbro), the application of stable isotopes is hampered since it does not lead to unequivocal results. Stable isotopes only lead to clear results if the water/rock ratios are relatively high. The same applies to mantle-like zircon $\delta^{18}O$ values, as analyzed

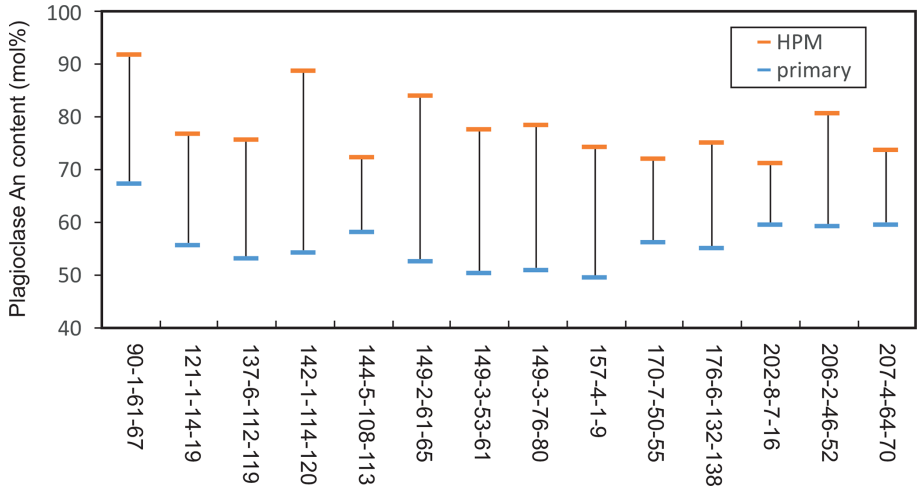

Figure 5. Compositions of primary and residual An-enriched (HPM) plagioclase in the investigated samples. The values of the primary crystals are averages, whereas the compositions of the An-enriched plagioclases are representative of the zones with the highest An content (see Table 1).

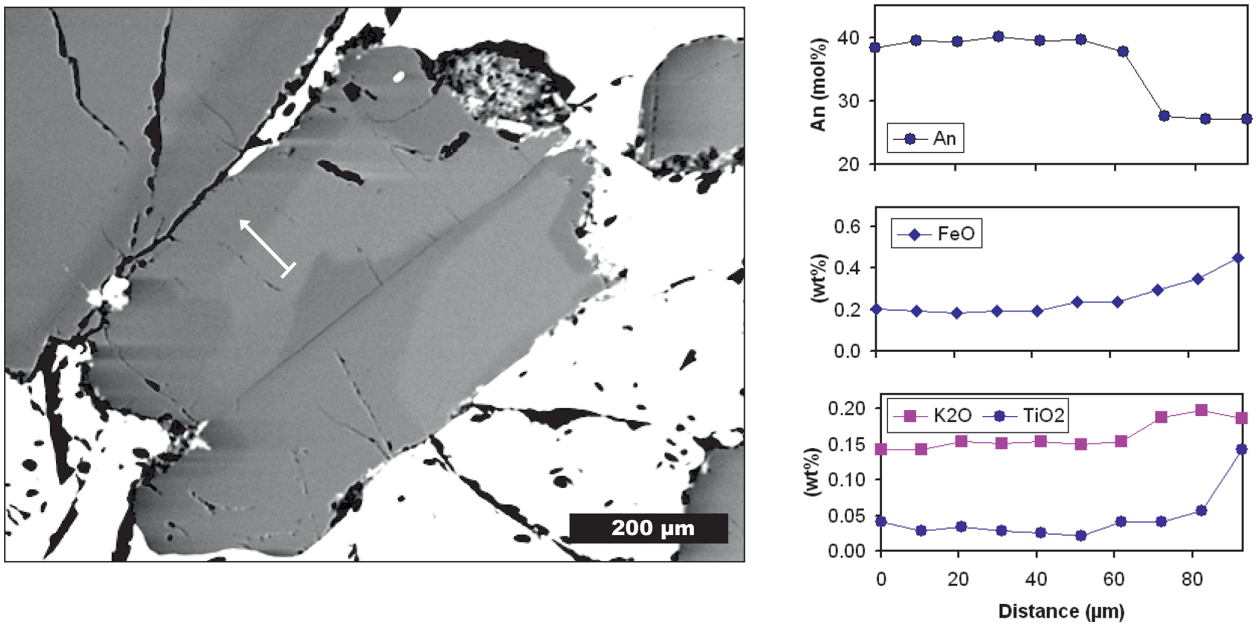

Figure 6. On the left is a BSE image of zoned plagioclases within a cluster of late-stage Fe–Ti oxides (white phases) in a ferrogabbro from the 735B drill core (sample 143-2-105-112). Note the different gray levels, which indicate different compositions: lighter-gray levels indicate higher An content in the cores, and darker-gray levels indicate lower An content in the rims. The line indicates the position of the microprobe profile shown on the right. The late melt, rich in Fe and Ti, reacted with the primary plagioclase, resulting in the dissolution of the primary plagioclase and the precipitation of a new, albite-rich plagioclase. Note that the latter plagioclase exhibits significantly higher TiO_2 and K_2O values, consistently with the observation that late melts evolve through fractional crystallization of MORB and are enriched in these elements.

by Zhang et al. (2025) for felsic veins from IODP Hole U1473. These values were interpreted as reflecting limited seawater involvement. However, as for bulk rocks, mantle-like zircon δ18O values do not rule out an origin from seawater-derived hydrous partial melting if the water/rock ratio is very low.

2. The presence of high concentrations of chlorine in amphiboles and apatites in magmatically formed rocks from the lower oceanic crust of mid-ocean ridges is widely accepted as evidence of the involvement of seawater-derived fluids in the formation process. Koepke et al. (2007) presented a model whereby partial

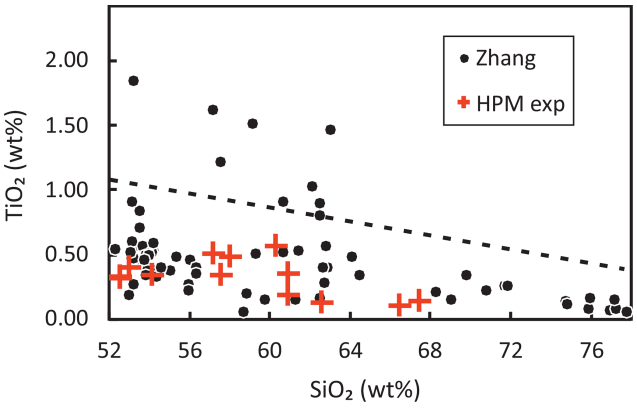

Figure 7. TiO_2 versus SiO_2 diagram showing the bulk data of published felsic veins from the ODP and IODP drill cores at Atlantis Bank, as well as experimental melts derived from hydrous partial melting of oceanic gabbros ("HPM experimental"; Koepke et al., 2004). The felsic veins are from the data compilation of Zhang et al. (2025; Supplementary Data 16). The line corresponds to the minimum TiO_2 values obtained from experiments on MORB differentiation in tholeiitic systems. This implies that melts below this line are most likely products of hydrous partial melting of gabbro rather than MORB differentiation (for details see Koepke et al., 2007).

melting of oceanic gabbros could be initiated by hot, seawater-derived hydrothermal fluids percolating along grain boundaries above the wet gabbro solidus. Clearly, the system gained a Cl input, which should be evident in phases that can incorporate Cl, such as brown amphiboles. As the amphiboles present in the microstructures investigated in this study have rather low Cl concentrations (see the Results section), it can be inferred that the fluids responsible for triggering partial melting are not derived from seawater. The analyzed Cl concentrations are similar to those of typical late-stage amphiboles in oceanic gabbros, which also generally have Cl contents below 0.02 wt % (e.g., Coogan et al., 2001). The same is true of amphiboles produced by simulating hydrous partial melting of gabbro experimentally with the addition of pure water, which have a Cl concentration below 0.02 wt % (Wolff et al., 2013). However, experiments performed in the same study using a seawater analogue instead of distilled water produced similar results, with Cl concentrations varying from 0.008 to 0.015 wt %. This shows that the low Cl content of the amphiboles analyzed in this study does not rule out the formation process being initiated by partial melting caused by fluids derived from seawater. It should be noted that amphibole Cl content is a complex function of fluid composition, temperature, pressure, and crystallographic factors (e.g., Manning and Aranovich, 2014).

Ferrando et al. (2022) examined brown amphiboles found in gabbros drilled from Hole U1473 to determine the nature of the fluid present. According to these authors, the low Cl content of brown amphiboles indicates that they crystallized from melts containing a magmatic hydrous component. This suggests that the microstructures of hydrous partial melting observed in the gabbros in this study could have been formed by magmatic fluids percolating through the gabbro at temperatures above its solidus. On the other hand, Zhang et al. (2025) highlighted the crucial role of detachment faulting in the lower ocean crust of the Atlantis Bank core complex in facilitating seawater-induced hydrous partial melting at temperatures exceeding 750 °C. In summary, the discovered microstructures in the gabbro drilled in Hole 735B clearly indicate that hydrous partial melting occurred in the gabbro. However, the origin of the water that triggered this process remains unclear.

4.3 What happens to the felsic melts?

The residual microstructures observed in the Hole-735B gabbros, which are indicative of hydrous partial melting, imply that felsic melts have been generated. However, interstitial phases representing frozen melt associated with the residual microstructures have never been observed, e.g., granular felsic leucosomes associated with quartz. Therefore, they were not frozen in situ, as is typical of high-grade metamorphic migmatite terrains in the deep continental crust. This raises the question: what happened to these melts? In the following section, two options are discussed.

1. An important fact is that the gabbros from the Atlantis Bank core complex generally crystallized in a tectonically active regime, as evidenced by crystal–plastic deformation (e.g., Dick et al., 2019; MacLeod et al., 2017). Therefore, it is highly probable that the felsic melts, which were generated in a ductile regime, migrated into zones with less pronounced deformation, where they finally solidified. These locations for crystallization include fractures or cracks within gabbroic rocks in a cooler, eventually brittle regime. This results in the formation of widespread felsic veins within the gabbro massif. It is also highly probable that the anatectic melts mix with late-stage vagabonding melts formed by extended crystal fractionation, producing hybrid melts that exhibit characteristics of both modes of felsic melt generation. Such mixing could be indicated by the compositions of magmatic amphiboles that crystallized within the felsic veins, which show moderate F and Cl contents. This is the case for some amphiboles within felsic veins from Hole U1473A in the Ma et al. (2020) data set.

2. At high temperatures and pressures, water-rich fluids have the potential to dissolve considerable amounts of rock components, especially quartz and alkali metals. According to Dolejs and Manning's (2010) thermodynamic model of mineral solubility in aqueous fluids, the solubility of quartz in pure water under conditions that

facilitate relevant anatectic processes within the ocean crust is approximately 2 wt %. Since the amount of melt generated by hydrous partial melting is considered to be very low, the dissolution and removal of anatectic melts by a water-rich fluid could be considered to be a reliable explanation for the absence of in situ frozen felsic melts (for details, see Koepke et al., 2014).

4.4 A model for the generation of felsic veins by hydrous partial melting of gabbro

The following outlines our model for the formation of interstitial, late-stage parageneses with zones of plagioclase strongly enriched in An content by partial melting of oceanic gabbro at slow-spreading ridges initiated by hydrothermal fluids; this is illustrated in Fig. 8. This model corresponds to the ideas of Zhang et al. (2025), who proposed seawater-involved hydrous partial melting for their group-1 felsic veins cutting gabbros in Hole U1473A. The process involves three distinct stages:

1. The first step is the main-stage crystallization of olivine, plagioclase, and clinopyroxene in the axial magma beneath the mid-ocean ridge. After accumulation, the cumulate cools into the subsolidus regime but remains above the wet solidus temperature of gabbro (Fig. 8a).

2. In a second stage, hydrothermal circulation at very high temperatures begins with the migration of water-rich fluids along grain boundaries, triggering the incongruent hydrous partial-melting reaction (Fig. 8b). In this model, the fluids originate from seawater.

3. In a third stage, the melting process on grain boundaries progresses. At plagioclase–plagioclase grain boundaries, new plagioclase highly enriched in An forms. At the edges of olivine and clinopyroxene, interstitial brown amphibole and/or orthopyroxene precipitate (Fig. 8c). It should be noted that an experimental study using gabbro microrocks as starting material (Wolff et al., 2013) has evidenced the kinetics of this reaction, including the evolution of the characteristic microstructures at grain boundaries between primary plagioclases and at the rims of olivine and/or clinopyroxene. This paper presents 14 gabbro samples from ODP drill core 735B, in which these microstructures have been observed (see the Supplement).

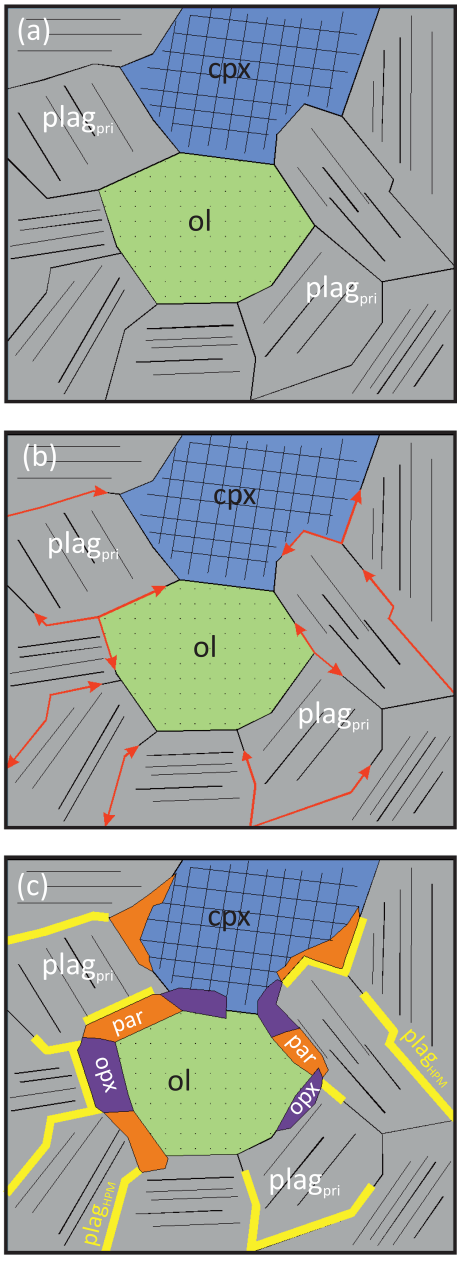

Figure 8. Schematic sketch showing the process of partial melting of oceanic gabbros by hydrothermal fluids percolating on grain boundaries. **(a)** Cumulate formation. The main-stage crystallization of olivine (ol), clinopyroxene (cpx), and primary plagioclase ($plag_{pri}$) forms a dry cumulate network, which cools down into the subsolidus regime. **(b)** Hydrothermal fluid migration. Water-rich fluids derived from seawater migrate above the wet gabbro solidus along grain boundaries (red arrows), initiating the incongruent partial-melting reaction. **(c)** Progress of hydrous partial melting on grain boundaries. At grain boundaries between primary plagioclases, new plagioclase strongly enriched in An is formed ($plag_{HPM}$; yellow zones). When these zones meet cumulate olivine and clinopyroxene, interstitial pargasitic amphibole (par) and/or orthopyroxene (opx) precipitate. Modified after Koepke et al. (2014).

5 Concluding remarks

Detailed petrographical and microanalytical investigations of gabbroic rocks from ODP drill core 735B, which was drilled on top of Atlantis Bank at the SWIR, reveal that many of these gabbros exhibit characteristic microstructures, indicating that they formed through hydrous partial melting of gabbro. The key features that led to this conclusion are the zones

of An-rich plagioclase on grain boundaries, which form parageneses with interstitial brown amphibole and orthopyroxene. These are interpreted as the residual phase assemblage left after a hydrous partial-melting event. This is fully consistent with experiments using gabbro microrocks as starting material, which revealed precisely the same microstructures as those observed in the SWIR gabbros (Wolff et al., 2013). Even microanalytical details, such as the strongly impoverished trace element concentrations in the An-enriched plagioclase (Ti, Mg, K), correspond to the experiments.

The microstructures found in the gabbros from Hole 735B clearly indicate that hydrous partial melting has occurred. However, this study does not examine the relationship between these melts and the felsic veins that cut through the Atlantis Bank gabbros. In order to do so, the veins themselves must be investigated. Zhang et al. (2025) demonstrated this by analyzing the trace element compositions of zircons found in the veins of Hole 1473A. They showed that both hydrous partial melting of gabbro and extreme fractional crystallization of MORB were involved in forming the felsic melts. The microstructures observed in the gabbros from Hole 735B indicate proceeded hydrous partial melting and support their statement.

Data availability. No data sets were used in this article.

Supplement. The supplement related to this article is available online at https://doi.org/10.5194/ejm-38-179-2026-supplement.

Competing interests. The author has declared that there are no competing interests.

Disclaimer. Publisher's note: Copernicus Publications remains neutral with regard to jurisdictional claims made in the text, published maps, institutional affiliations, or any other geographical representation in this paper. The authors bear the ultimate responsibility for providing appropriate place names. Views expressed in the text are those of the authors and do not necessarily reflect the views of the publisher.

Acknowledgements. We acknowledge the Chief Editor, Elisabetta Rampone; the Associate Editor, Riccardo Tribuzio; Tomoaki Morishita; and an anonymous reviewer for their constructive comments and valuable suggestions that helped to improve the paper. Otto Diedrichs's careful thin-section preparation and Andreas Moeller's (University of Kansas) help during CL operation at the University Potsdam are gratefully acknowledged. This research used samples and/or data provided by the Ocean Drilling Program (ODP). ODP is sponsored by the US National Science Foundation (NSF) and participating countries under the management of the Joint Oceanographic Institutions (JOI), Inc.

Financial support. This research has been supported by the Deutsche Forschungsgemeinschaft (grant no. KO 1723/7-1,2).

The publication of this article was funded by the open-access fund of Leibniz Universität Hannover.

Review statement. This paper was edited by Riccardo Tribuzio and reviewed by Tomoaki Morishita and one anonymous referee.

References

Berndt, J., Liebske, C., Holtz, F., Freise, M., Nowak, M., Ziegenbein, D., Hurkuck, D., and Koepke, J.: A combined rapid-quench and H2-membrane setup for internally heated pressure vessels: Description and application for water solubility in basaltic melts, Am. Mineral., 87, 1717–1726, 2002.

Berndt, J., Koepke, J., and Holtz, F.: An experimental investigation of the influence of water and oxygen fugacity on differentiation of MORB at 200 MPa, J. Petrol., 46, 135–167, 2005.

Bosch, D., Jamais, M., Boudier, F., Nicolas, A., Dautria, J.-M., and Agrinier, P.: Deep and high-temperature hydrothermal circulation in the Oman ophiolite – Petrological and isotopic evidence, J. Petrol., 45, 1181–1208, 2004.

Boulanger, M., France, L., Ferrando, C., Ildefonse, B., Ghosh, B., Sanfilippo, A., Liu, C. Z., Morishita, T., Koepke, J., and Bruguier, O.: Magma-Mush Interactions in the Lower Oceanic Crust: Insights From Atlantis Bank Layered Series (Southwest Indian Ridge), J. Geophys. Res.-Sol. Ea., 126, https://doi.org/10.1029/2021jb022331, 2021.

Brophy, J. G. and Pu, X. F.: Rare earth element-SiO_2 systematics of mid-ocean ridge plagiogranites and host gabbros from the Fournier oceanic fragment, New Brunswick, Canada: a field evaluation of some model predictions, Contrib. Mineral. Petrol., 164, 191–204, https://doi.org/10.1007/s00410-012-0732-x, 2012.

Chen, Y. H., Niu, Y. L., Wang, X. H., Gong, H. M., Guo, P. Y., Gao, Y. J., and Shen, F. Y.: Petrogenesis of ODP Hole 735B (Leg 176) Oceanic Plagiogranite: Partial Melting of Gabbros or Advanced Extent of Fractional Crystallization?, Geochem. Geophy. Geosy., 20, 2717–2732, https://doi.org/10.1029/2019gc008320, 2019.

Coogan, L. A.: The lower oceanic crust; 2nd edn., Treatise on Geochemistry, edited by: Turekian, K., and Holland, H. D., Elsevier, Amsterdam, 497–541, https://doi.org/10.1016/B978-0-08-095975-7.00315-6, 2014.

Coogan, L. A., Wilson, R. N., Gillis, K. M., and MacLeod, C. J.: Near-solidus evolution of oceanic gabbros: Insights from amphibole geochemistry, Geochim. Cosmochim. Ac., 65, 4339–4357, 2001.

Dhar, A., Ghosh, B., Bandyopadhyay, D., Morishita, T., Tamura, A., France, L., Nguyen, D. K., Boulanger, M., Koley, M., Roy, S., and Chattopadhaya, S.: The lower oceanic crust at ultraslow-spreading Southwest Indian Ridge: The inside story, Gondwana Res., 111, 223–248, https://doi.org/10.1016/j.gr.2022.08.008, 2022.

Dick, H. J. B., MacLeod, C.J., Blum, P., and the Expedition 360 Scientists: Expedition 360 Preliminary Report: Southwest Indian Ridge lower crust and Moho. International Ocean Discovery Program, 50 pp., https://doi.org/10.14379/iodp.pr.360.2016, 2016.

Dick, H. J. B., Natland, J. H., Alt, J. C., Bach, W., Bideau, D., Gee, J. S., Haggas, S., Hertogen, J. G. H., Hirth, G., Holm, P. M., Ildefonse, B., Iturrino, G. J., John, B. E., Kelley, D. S., Kikawa, E., Kingdon, A., LeRoux, P. J., Maeda, J., Meyer, P. S., Miller, D. J., Naslund, H. R., Niu, Y. L., Robinson, P. T., Snow, J., Stephen, R. A., Trimby, P. W., Worm, H. U., and Yoshinobu, A.: A long in situ section of the lower ocean crust: results of ODP Leg 176 drilling at the Southwest Indian Ridge, Earth Planet. Sci. Lett., 179, 31–51, 2000.

Dick, H. J. B., Ozawa, K., Meyer, P. S., Niu, Y., Robinson, P. T., Constantin, M., Hebert, R., Maeda, J., Natland, J. H., Hirth, J. G., and Mackie, S. M.: Primary silicate mineral chemistry of a 1.5-km section of very slow spreading lower ocean crust: ODP Hole 735B, Southwest Indian Ridge, Proc. ODP, Sci. Results, 176, Chap. 10, 61 pp., https://www-odp.tamu.edu/publications/176_SR/VOLUME/CHAPTERS/SR176_10.PDF (last access: 17 March 2026), 2002.

Dick, H. J. B., MacLeod, C. J., Blum, P., Abe, N., Blackman, D. K., Bowles, J. A., Cheadle, M. J., Cho, K., Ciazela, J., Deans, J. R., Edgcomb, V. P., Ferrando, C., France, L., Ghosh, B., Ildefonse, B., John, B., Kendrick, M. A., Koepke, J., Leong, J. A. M., Liu, C., Ma, Q., Morishita, T., Morris, A., Natland, J. H., Nozaka, T., Pluemper, O., Sanfilippo, A., Sylvan, J. B., Tivey, M. A., Tribuzio, R., and Viegas, G.: Dynamic Accretion Beneath a Slow-Spreading Ridge Segment: IODP Hole 1473A and the Atlantis Bank Oceanic Core Complex, J. Geophys. Res.-Sol. Ea., 124, 12631–12659, https://doi.org/10.1029/2018jb016858, 2019.

Dolejs, D. and Manning, C. E.: Thermodynamic model for mineral solubility in aqueous fluids: theory, calibration and application to model fluid-flow systems, Geofluids, 10, 20–40, 2010.

Ernst, W. G. and Liu, J.: Experimental phase-equilibrium study of Al- and Ti-contents of calcic amphibole in MORB – a semiquantitative thermobarometer, Am. Mineral., 83, 952–969, 1998.

Ferrando, C., Basch, V., Ildefonse, B., Deans, J., Sanfilippo, A., Barou, F., and France, L.: Role of compaction in melt extraction and accumulation at a slow spreading center: Microstructures of olivine gabbros from the Atlantis Bank (IODP Hole U1473A, SWIR), Tectonophysics, 815, https://doi.org/10.1016/j.tecto.2021.229001, 2021.

Ferrando, C., Tribuzio, R., Lissenberg, C. J., France, L., MacLeod, C. J., Basch, V., Villeneuve, J., Deloule, E., and Sanfilippo, A.: Brown Amphibole as Tracer of Tectono-Magmatic Evolution of the Atlantis Bank Oceanic Core Complex (IODP Hole U1473A), J. Petrol., 63, https://doi.org/10.1093/petrology/egac089, 2022.

Flagler, P. A. and Spray, J. G.: Generation of plagiogranite by amphibolite anatexis in oceanic shear zones, Geology, 19, 70–73, 1991.

Johannes, W. and Holtz, F.: Petrogenesis and experimental petrology of granitic rocks, Minerals and rocks, Springer, Berlin, Heidelberg, 22, 335 pp., https://doi.org/10.1093/petroj/38.1.165, 1996.

Kendrick, M. A.: Halogens in Atlantis Bank gabbros, SW Indian Ridge: Implications for styles of seafloor alteration, Earth Planet. Sci. Lett., 514, 96–107, https://doi.org/10.1016/j.epsl.2019.02.034, 2019.

Koepke, J., Feig, S. T., Snow, J., and Freise, M.: Petrogenesis of oceanic plagiogranites by partial melting of gabbros: An experimental study, Contrib. Mineral. Petrol., 146, 414–432, 2004.

Koepke, J., Feig, S. T., and Snow, J.: Late-stage magmatic evolution of oceanic gabbros as a result of hydrous partial melting: Evidence from the ODP Leg 153 drilling at the Mid-Atlantic Ridge, Geochem. Geophy. Geosy., 6, 2004GC000805, pp. 000801-000827, 2005a.

Koepke, J., Feig, S. T., and Snow, J.: Hydrous partial melting within the lower oceanic crust, Terra Nova, 17, 286–291, 2005b.

Koepke, J., Berndt, J., Feig, S. T., and Holtz, F.: The formation of SiO_2-rich melts within the deep oceanic crust by hydrous partial melting of gabbros, Contrib. Mineral. Petrol., 153, 67–84, 2007.

Koepke, J., Berndt, J., Horn, I., Fahle, J., and Wolff, P. E.: Partial melting of oceanic gabbro triggered by propagating water-rich fluids: a prime example from the Oman ophiolite, in: Tectonic Evolution of the Oman Mountains., edited by: Rollinson, H. R., Searle, M. P., Abbasi, I. A., Al-Lazki, A., and Al-Kindi, M. H., Geological Society of London, Special Publication, London, 392, 187–204, 2014.

Koepke, J., Botcharnikov, R., and Natland, J. H.: Crystallization of late-stage MORB under varying water activities and redox conditions: Implications for the formation of highly evolved lavas and oxide gabbro in the ocean crust, Lithos, https://doi.org/10.1016/j.lithos.2018.10.001, 2018.

Locock, A. J.: An Excel spreadsheet to classify chemical analyses of amphiboles following the IMA 2012 recommendations, Comput. Geosci., 62, 1–11, https://doi.org/10.1016/j.cageo.2013.09.011, 2014.

Ma, Q., Dick, H. J. B., Urann, B., and Zhou, H. Y.: Silica-Rich Vein Formation in an Evolving Stress Field, Atlantis Bank Oceanic Core Complex, Geochem. Geophy. Geosy., 21, https://doi.org/10.1029/2019gc008795, 2020.

MacLeod, C. J., Dick, H. J. B., Blum, P., and the Expedition 360 Scientists: Southwest Indian Ridge Lower Crust and Moho, Proceedings of the Integrated Ocean Drilling Program, 360, https://doi.org/10.14379/iodp.proc.360.103.2017, 2017.

Manning, C. E. and Aranovich, L. Y.: Brines at high pressure and temperature: Thermodynamic, petrologicand geochemical effects, Precambrian Res., 253, https://doi.org/10.1016/j.precamres.2014.06.025, 2014.

Natland, J. H., Meyer, P. S., Dick, H. J. B., and Bloomer, S. H.: Magmatic oxides and sulfides in gabbroic rocks from ODP Hole 735B and the later development of the liquid line of descent, in: Proc. ODP, Sci. Results, edited by: Von Herzen, R. P., Fox, J., Palmer-Julson, A., and Robinson, P. T., Ocean Drilling Program, College Station, TX, 118, 41–73, https://doi.org/10.2973/odp.proc.sr.118.163.1991, 1991.

Nguyen, D. K., Morishita, T., Soda, Y., Tamura, A., Ghosh, B., Harigane, Y., France, L., Liu, C. Z., Natland, J. H., Sanfilippo, A., MacLeod, C. J., Blum, P., and Dick, H. J. B.: Occurrence of Felsic Rocks in Oceanic Gabbros from IODP Hole U1473A: Implications for Evolved Melt Migration in the Lower Oceanic Crust, Minerals, 8, 583, https://doi.org/10.3390/min8120583, https://doi.org/10.3390/min8120583, 2018.

Niu, Y., Gilmore, T., Mackie, S., Greig, A., and Bach, W.: Mineral chemistry, whole-rock compositions, and petrogenesis of Leg 176 gabbros: data and discussion, in: Proc. ODP, Sci. Results, edited by: Natland, J. H., Dick, H. J. B., Miller, D. J., and Von Herzen, R. P., Ocean Drilling Program, College Station, TX, 1–60, 2002.

Pietranik, A., Storey, C., Koepke, J., and Lasalle, S.: Zircon record of fractionation, hydrous partial melting and thermal gradients at different depths in oceanic crust (ODP Site 735B, South-West Indian Ocean), Contrib. Mineral. Petrol., 172, 10, https://doi.org/10.1007/s00410-016-1324-y, 2017.

Pouchou, J. L. and Pichoir, F.: Quantitative analysis of homogeneous or stratified microvolumes applying the model "PAP", in: Electron probe quantification, edited by: Heinrich, K. F. J. and Newbury, D. E., Plenum Press, New York, 31–75, https://doi.org/10.1007/978-1-4899-2617-3, 1991.

Sanfilippo, A., MacLeod, C. J., Tribuzio, R., Lissenberg, C. J., and Zanetti, A.: Early-Stage Melt-Rock Reaction in a Cooling Crystal Mush Beneath a Slow-Spreading Mid-Ocean Ridge (IODP Hole U1473A, Atlantis Bank, Southwest Indian Ridge), Frontiers in Earth Science, 8, https://doi.org/10.3389/feart.2020.579138, https://doi.org/10.3389/feart.2020.579138, 2020.

Sisson, T. W. and Grove, T. L.: Experimental investigations of the role of H2O in calc-alkaline differentiation and subduction zone magmatism, Contrib. Mineral. Petrol., 113, 143–166, 1993.

Wolff, P. E., Koepke, J., and Feig, S. T.: The reaction mechanism of fluid-induced partial melting of gabbro in the oceanic crust, Eur. J. Mineral., 25, 279–298, https://doi.org/10.1127/0935-1221/2013/0025-2314, 2013.

Zhang, W. Q., Liu, C. Z., and Dick, H. J. B.: Evidence for Multi-stage Melt Transport in the Lower Ocean Crust: the Atlantis Bank Gabbroic Massif (IODP Hole U1473A, SW Indian Ridge), J. Petrol., 61, https://doi.org/10.1093/petrology/egaa082, 2020.

Zhang, W. Q., Liu, C. Z., Macleod, C. J., and Lissenberg, C. J.: The role of detachment faulting in the genesis of oceanic felsic melts, Communications Earth & Environment, 6, https://doi.org/10.1038/s43247-025-02098-3, 2025.